Journal of Nuclear Medicine, published on April 28, 2023 as doi:10.2967/jnumed.122.265254

Comparative Evaluation of [^{18}F]5-Fluoroaminosuberic Acid and (4*S*)-4-3-[^{18}F]fluoropropyl)-L-Glutamate as System x_C^-–Targeting Radiopharmaceuticals

Milena Colovic[1,2], Hua Yang[1], Lily Southcott[1], Helen Merkens[2], Nadine Colpo[2], Francois Bénard[2,3], and Paul Schaffer[1,3,4]

[1]*Life Sciences Division, TRIUMF, Vancouver, British Columbia, Canada;* [2]*Department of Molecular Oncology, BC Cancer Research Institute, Vancouver, British Columbia, Canada;* [3]*Department of Radiology, University of British Columbia, Vancouver, British Columbia, Canada; and* [4]*Department of Chemistry, Simon Fraser University, Burnaby, British Columbia, Canada*

System x_C^- is an appealing biomarker for targeting oxidative stress with oncologic PET imaging and can serve as an alternative PET biomarker to other metabolic indicators. In this paper, we report a direct comparison of 2 ^{18}F-labeled amino acid radiopharmaceuticals targeting system x_C^-, [^{18}F]5-fluoroaminosuberic acid ([^{18}F]FASu) and (4*S*)-4-(3-[^{18}F]fluoropropyl)-L-glutamate ([^{18}F]FSPG), in terms of their uptake specificity and ability to image glioma and lung cancer xenografts in vivo. **Methods:** Both tracers were synthesized according to previously published procedures. In vitro uptake specificity assays were conducted using prostate (PC-3), glioblastoma (U-87), colorectal (HT-29), ovarian (SKOV3), breast (MDA-MB-231), and lung cancer (A549) cell lines. PET/CT imaging and biodistribution studies were conducted in immunocompromised mice bearing U-87 or A549 xenografts. **Results:** In vitro cell uptake assays showed that the tracers accumulated in cancer cells in a time-dependent manner and that the uptake of [^{18}F]FASu was blocked by the system x_C^- inhibitor sulfasalazine and rose bengal, but not by system L inhibitor 2-aminobicyclo-(2,2,1)-heptane-2-carboxylic acid, system x_{AG}^- inhibitor L-*trans*-pyrrolidine-2,4-dicarboxylic acid, or L-serine, which is a substrate for transporter systems A, ACS, B^0, and $B^{0,+}$. Conversely, [^{18}F]FSPG uptake decreased significantly in the presence of an excess of L-*trans*-pyrrolidine-2,4-dicarboxylic acid in 2 of 3 tested cell lines, indicating some reliance on system x_{AG}^- in these cells. In an in vivo setting, [^{18}F]FASu and [^{18}F]FSPG generated good-contrast PET images in U-87 and A549 tumor–bearing mice. Tracer accumulation in A549 tumors was 5.0 ± 0.8 percentage injected dose (%ID)/g ([^{18}F]FASu, $n \geq 5$) and 6.3 ± 1.3 %ID/g ([^{18}F]FSPG, $n \geq 6$, $P = 0.7786$), whereas U-87 xenografts demonstrated uptake of 6.1 ± 2.4 %ID/g ([^{18}F]FASu, $n \geq 4$) and 11.2 ± 4.1 %ID/g ([^{18}F]FSPG, $n \geq 4$, $P = 0.0321$) at 1 h after injection. **Conclusion:** [^{18}F]FSPG had greater in vitro uptake than [^{18}F]FASu in all cell lines tested; however, our results indicate that residual uptake differences exist between [^{18}F]FSPG and [^{18}F]FASu, suggesting alternative transporter activity in the cell lines tested. In vivo studies demonstrated the ability of both [^{18}F]FASu and [^{18}F]FSPG to image glioblastoma (U-87) and non–small cell lung cancer (A549) xenografts.

Key Words: system x_C^- transporter; tumor imaging; amino acid tracer; ^{18}F; rose bengal

J Nucl Med 2023; 00:1–8
DOI: 10.2967/jnumed.122.265254

Oxidative stress (OS), resulting from the imbalance between the production of reactive oxygen species and their elimination by antioxidants (*1*), has been implicated in the metabolic reprogramming of cancer cells, causing them to become less sensitive to high levels of reactive oxygen species than normal cells (*1,2*). System x_C^- is a transmembrane transporter protein playing a partial role in this process through its action as the primary importer of intracellular cystine (*3*), which on entry into the cell is reduced to cysteine, the rate-limiting precursor in the biosynthesis of glutathione (*2*). Glutathione is vital for the maintenance of cellular redox balance and protection from OS (*4,5*). Consequently, system x_C^- is upregulated under OS and is found to be overexpressed in several different malignancies, including breast, pancreatic, and brain cancers (*6–8*). As a result, system x_C^- has emerged as a promising target in PET imaging, with several ^{18}F or ^{11}C radiopharmaceuticals reported to target system x_C^- to date (*9–14*). Among them, [^{18}F]5-fluoro-ASu ([^{18}F]FASu) and (4*S*)-4-(3-[^{18}F]fluoropropyl)-L-glutamate ([^{18}F]FSPG) are the most studied (Figs. 1A and 1B). [^{18}F]FSPG, a glutamate analog that demonstrated specific tumor uptake, is currently under evaluation in multiple multicenter clinical trials to determine its efficacy in detection and staging of various types of cancer, including, but not limited to, colorectal, breast, pulmonary, abdominal, and head and neck neoplasms (*15*). [^{18}F]FASu has been used in preclinical evaluations of breast cancer, lung cancer, and glioblastoma (*16,17*). Both tracers demonstrated the ability to target tumors with good specificity and contrast.

Herein, we report a comparative preclinical evaluation of 2 system x_C^-–imaging agents, [^{18}F]FASu and [^{18}F]FSPG, in tumor accumulation and specificity toward x_C^-. The comparison study was performed in non–small cell lung cancer (A549) and glioblastoma (U-87) cell lines and xenograft-bearing mice.

MATERIALS AND METHODS

Chemicals and Instrumentation

All chemicals and solvents were obtained from commercial sources and used without further purification. The quantity of injected radiofluorinated tracers was measured using a Capintec CRC-25R/W dose calibrator, and the radioactivity of mouse tissues collected from biodistribution studies was counted using a Perkin Elmer Wizard 2480 γ-counter. PET imaging experiments were conducted using an Inveon multimodality small-animal PET/CT system (Siemens Healthineers).

Received Dec. 5, 2022; revision accepted Mar. 21, 2023.
For correspondence or reprints, contact Paul Schaffer (pschaffer@triumf.ca).
Published online Apr. 27, 2023.

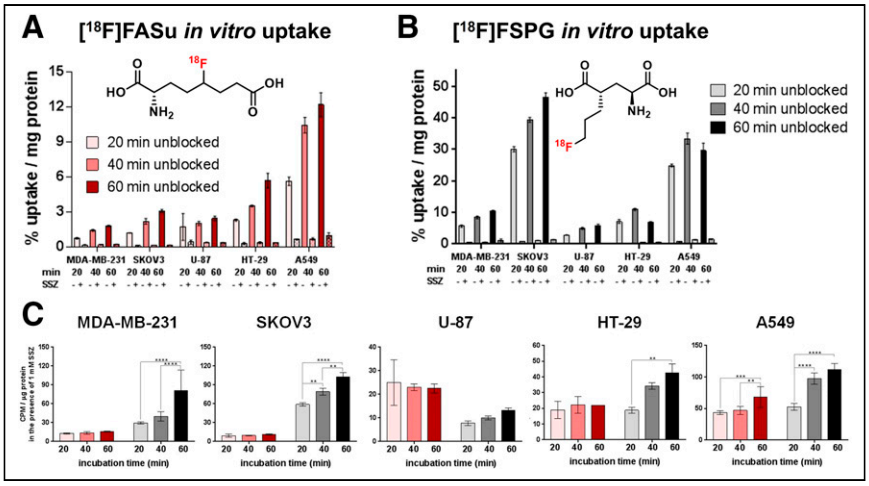

FIGURE 1. (A) [^{18}F]FASu in vitro uptake at 20, 40, and 60 min in absence and presence of xCT inhibitor sulfasalazine (1 mM). (B) [^{18}F]FSPG in vitro uptake at 20, 40, and 60 min in absence and presence of 1 mM sulfasalazine. Radiotracer structures are embedded into graphs. (C) [^{18}F]FASu and [^{18}F]FSPG in vitro uptake in presence of sulfasalazine (1 mM). Cells were incubated with tracer (red bars for [^{18}F]FASu, black bars for [^{18}F]FSPG) for 20, 40, or 60 min. Sulfasalazine was coadded with tracer. All uptake values are normalized to protein concentration and presented as percentage uptake per minute per milligram of protein (A and B) or as counts per minute per microgram of protein (C). SSZ = sulfasalazine. $^{*}P < 0.05$. $^{**}P < 0.01$. $^{***}P < 0.001$. $^{****}P < 0.0001$.

[^{18}F]FASu Synthesis

[^{18}F]FASu was synthesized as previously reported (*18*), with a minor change in formulation. The supplemental materials provide further details (available at http://jnm.snmjournals.org). The original [^{18}F]FASu formulation used a trifluoroacetic acetate counterion, but for this study, we used a tracer formulated with a chloride counterion. This change was implemented to match formulations between [^{18}F]FASu and [^{18}F]FSPG. Our validation biodistribution studies indicated no statistically significant differences in biodistribution of [^{18}F]FASu based on the formulation used (Supplemental Fig. 1). Decay-corrected radiochemical yield (d.c. RCY) was 18 ± 6% (n = 6), radiochemical purity was greater than 98%, and molar activity was 17.5 ± 7 GBq/mmol (n = 6).

[^{18}F]FSPG Synthesis

[^{18}F]FSPG was synthesized as previously reported (*12*). The final product was purified by an SCX cation exchange column and taken up in phosphate-buffered saline buffer. The decay-corrected radiochemical yield was 28 ± 7% (n = 4), radiochemical purity was greater than 98%, and molar activity was 15 ± 5 GBq/mmol (n = 4).

In Vitro Uptake Specificity Studies

All cell lines used in this study were authenticated by DDC Medical.

For tracer uptake and competition studies, the tumor cells were seeded in 24-well plates at appropriate concentrations. The cell number used for seeding was adjusted for every tumor cell line to yield approximately 200,000 cells per well on the day of the uptake study. Cells were usually grown for 2–3 d under standard conditions (37°C, 5% CO_2) until subconfluency. The cell number on the day of the uptake assay was determined by detaching cells in 3 representative wells and counting the cells using the MOXI Z mini automated cell counter kit (Orflo). Uptake data were normalized to 100,000 cells or per the protein content in representative wells.

Before the radioactive uptake assay, the cell culture medium was removed, and the cells were washed twice with *N*-(2-hydroxyethyl)piperazine-*N*′-(2-ethanesulfonic acid) basal salt solution buffer. Radiotracers were added to the assay buffer using 148 kBq per well. For competition experiments, the cells were coincubated with competitors either in excess at 1 mM or in a dose-dependent manner (0.001–1 mM). Tracer uptake was stopped by removal of the assay buffer at the indicated time points. Cells were quickly washed twice with 400 μL of ice-cold *N*-(2-hydroxyethyl)-piperazine-*N*′-(2-ethanesulfonic acid) basal salt solution buffer and lysed with the addition of 1 M NaOH. The cell lysate was removed from the plates. Radioactivity of ^{18}F samples was determined using a γ-counter.

Animal Studies

All animal experiments were conducted in accordance with the guidelines established by the Canadian Council on Animal Care and approved by the Animal Ethics Committee of the University of British Columbia. Immunodeficient 129S6/SvEvTac-*Rag2*^{tm1Fwa} (Rag2M) mice were bred in-house at the Animal Research Centre, British Columbia Cancer Research Institute, and used in this study. Food and water were provided ad libitum for the entire duration of the study.

Tumor Inoculation

Mice were anesthetized briefly with 2.5% isoflurane in oxygen, 2.0 L/min, during cell implantation. After the upper back area below the left shoulder was shaved, the injection site was wiped with an alcohol prep pad, and a 28.5-gauge needle was used to subcutaneously inject approximately 5 × 10^6 U-87 cells or approximately 2 × 10^6 A549 cells (in 100 μL 1× phosphate-buffered saline and BD Matrigel Matrix at a 1:1 ratio). Biodistribution studies and PET/CT imaging were performed when tumors reached 5–7 mm in diameter.

Biodistribution Studies

Tumor-bearing mice were briefly anesthetized with isoflurane inhalation and injected with 0.9–2.5 MBq of [^{18}F]FASu or [^{18}F]FSPG (100–200 μL in saline, intravenously). The mice were allowed to roam freely in their cages for 1 h and were then killed by CO_2 asphyxiation. Their blood was promptly harvested by cardiac puncture. Organs or tissues of interest were collected in a subsequent necropsy, washed with phosphate-buffered saline, blotted dry, and weighed, and their activity was counted, normalized to the injected dose, and expressed as the percentage injected dose per gram of tissue (%ID/g).

PET Imaging and Data Analysis

Anesthetized mice were injected with 3.94–5.22 MBq through the caudal vein. A 10-min CT scan was performed, followed by a 15-min static or 60-min dynamic PET acquisition on the small-animal PET/CT scanner. PET data were acquired in list mode. After the static acquisition at 1 h after injection, the mice were killed by CO_2 asphyxiation, followed by cardiac puncture. The tissues of interest were harvested, weighed, and counted on the γ-counter. The PET data were reconstructed using the 3-dimensional ordered-subset expectation maximization (2 iterations) maximum a priori (18 iterations) algorithm with CT-based attenuation correction. Inveon Research Workplace software (Siemens Healthineers) was used for image analysis and drawing 3-dimensional regions of interest to determine the %ID/g of tissue for selected organs. In addition, Inveon Research Workplace software was used to generate maximum-intensity projection images for visualization.

Statistical Analysis

All data are expressed as mean ± SD. Statistical analysis was performed using GraphPad (7.0-h) software. Two-way ANOVA analysis was performed for all tracer comparisons for in vitro and biodistribution studies. Multiple comparisons were corrected using the Šidak method. Student *t* tests were performed for all organs and tumor-to-organ ratios in the biodistribution blocking studies. The difference was considered statistically significant at a *P* value of less than 0.05.

RESULTS

In Vitro Cell Uptake Studies

Uptake of both [^{18}F]FASu and [^{18}F]FSPG was measured in 5 different human cancer cell lines: MDA-MB-231 (breast), U-87 (glioblastoma), HT-29 (colorectal), A549 (lung), and SKOV3 (ovarian). The uptake generally increased over time and was blocked by the system x_C^- inhibitor sulfasalazine (1 mM) in all cases (Figs. 1A and 1B). [^{18}F]FSPG had greater uptake overall, with U-87 cells retaining 5.8% ± 0.5% activity/mg of protein at 60 min and A549 and SKOV3 exceeding 29.6% ± 2.4% uptake/mg of protein (Fig. 1B). [^{18}F]FASu uptake was also inhibited by the addition of sulfasalazine in all cell lines studied (Fig. 1A); however, the activity taken up by the cells in the absence of sulfasalazine ranged from 1.8% ± 0.1% uptake/mg of protein to 12.2% ± 1.0% uptake/mg of protein at 60 min in A549 cells. Figure 1C illustrates uptake values in the presence of excess sulfasalazine, where it is evident that the uptake of the 2 tracers no longer differed by severalfold, in all cell lines except SKOV3. Furthermore, we observed that the uptake of [^{18}F]FASu in the presence of 1 mM sulfasalazine did not change with increasing incubation time, except in A549 cells, where it increased from 0.650% ± 0.042% uptake/mg of protein at 20 min to 0.988% ± 0.242% uptake/mg of protein at 60 min ($P < 0.0001$). Under the same conditions, [^{18}F]FSPG uptake continued increasing with prolonged incubation in all cell lines despite the presence of 1 mM sulfasalazine, with the exception of U-87 cells, which demonstrated no significant change over time ($P = 0.7069$ for 20- vs. 60-min comparison and $P > 0.89$ for 20- vs. 40-min and 40- vs. 60-min comparisons; Fig. 1C).

In vitro specificity assays were performed in A549, U-87, and MDA-MB-231 cell lines using the system x_C^- inhibitor sulfasalazine and inhibitors of the excitatory amino acid transporter protein (EAAT) family of transporters (L-*trans*-pyrrolidine-2,4-dicarboxylic acid [PDC]) (*19*) of vesicular glutamate transporters (rose bengal) (*20*) and of system L transporter (2-aminobicyclo-[2,2,1]-heptane-2-carboxylic acid) (*21–23*), in addition to L-serine, which is a known substrate of transporter systems A, ASC, B^0, and asc (*24*). Once again, sulfasalazine significantly inhibited uptake of both [^{18}F]FASu and [^{18}F]FSPG ($P < 0.05$ for each comparison, $n = 3$; Fig. 2; Supplemental Fig. 2). [^{18}F]FASu uptake was not significantly inhibited in the presence of excess PDC, L-serine, or 2-aminobicyclo-[2,2,1]-heptane-2-carboxylic acid (*P* value varied but exceeded 0.463 for each comparison). Conversely, [^{18}F]FSPG uptake decreased significantly in the presence of excess PDC in A549 and MDA-MB-231 cells ($P = 0.0006$ and $P = 0.0002$, respectively, equivalent to 26.7% and 28.7% uptake inhibition), but not in the U-87 cell line ($P = 0.4570$, corresponding to 8.9% uptake inhibition), which indicated possible involvement of EAATs in these cell lines. This finding is consistent with those of Koglin et al. and Greenwood et al., who also reported competition of [^{18}F]FSPG uptake with both aspartate and glutamate, which are the natural substrates of the EAATs (*12,24*). Moreover, we observed significant uptake blocking in the presence of L-serine in all 3 cell lines ($P = 0.0047$ for A549, $P = 0.0340$ for U-87, and $P = 0.0001$ for MDA-MB-231 cells, equivalent to 21.7%, 17.0%, and 40.2% [^{18}F]FSPG uptake inhibition, respectively). We also found that the most potent vesicular glutamate transporter inhibitor, rose bengal (*25*), inhibited the uptake of both [^{18}F]FASu and [^{18}F]FSPG (*P* value varied but was ≤0.0015 for each comparison) and that it had better blocking efficacy than sulfasalazine in the case of both tracers and across all cell lines studied (Fig. 2; Supplemental Fig. 3). Western blotting indicated expression of EAAT3 and EAAT4 transporters in U-87 and MDA-MB-231 whole-cell lysates (Supplemental Fig. 4). Furthermore, blotting of EAAT1 and EAAT2 indicated bands corresponding to the expression of glycosylated proteins, causing a band shift of 5–15 kDa (*26*), as well as detection of EAAT1 homodimers and homotrimers in all 3 cell lines tested.

The affinity of [^{18}F]FASu and [^{18}F]FSPG to system x_C^- transporter was further studied in a dose-dependent manner in competition assays

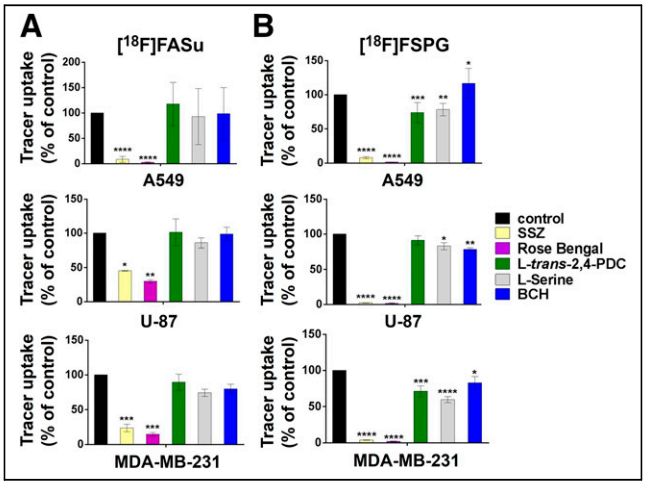

FIGURE 2. Two-way ANOVA analysis of 1-h uptake of [^{18}F]FASu (A) and [^{18}F]FSPG (B) in A549, U-87, and MDA-MB-231 cells, expressed as percentage of control sample uptake. BCH = 2-aminobicyclo-(2,2,1)-heptane-2-carboxylic acid. *$P < 0.05$. **$P < 0.01$. ***$P < 0.001$. ****$P < 0.0001$.

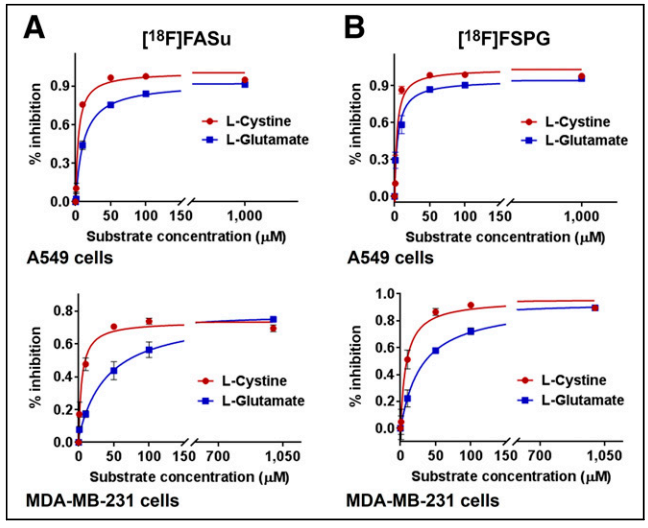

FIGURE 3. Dose-dependent competition cell uptake assays were performed in A549 (top) and MDA-MB-231 (bottom) cells using 148 kBq per well of either [^{18}F]FASu (A) or [^{18}F]FSPG (B) and increasing concentration of L-cystine or L-glutamate.

TABLE 1
Half-Maximal Inhibitory Concentrations (μM) from Tracer Competition Uptake Assays Against L-Cystine and L-Glutamate

Substrate	Cell line	[^{18}F]FASu (±SE)	[^{18}F]FSPG (±SE)
L-Cystine	A549	3.92 ± 0.60	3.23 ± 1.01
L-Glutamate	A549	10.93 ± 1.00	5.20 ± 1.18
L-Cystine	MDA-MB-231	4.56 ± 0.89	7.88 ± 1.36
L-Glutamate	MDA-MB-231	41.01 ± 6.32	29.29 ± 3.60

Assays were performed in A549 and MDA-MB-231 cells (n = 3).

against the natural substrates of system x_C^-: L-cystine and L-glutamate. Half-maximal inhibitory concentrations of 3.92 ± 0.60 and 3.23 ± 1.01 μM were determined for L-cystine in competition with [^{18}F]FASu and [^{18}F]FSPG, respectively, in A549 cells (Fig. 3; Table 1). These values are less than the values determined in competition with L-glutamate: 10.93 ± 1.00 μM for [^{18}F]FASu and 5.20 ± 1.18 μM for [^{18}F]FSPG. Although the difference in half-maximal inhibitory concentrations for L-cystine was not significant (P = 0.6503), the L-glutamate half-maximal inhibitory concentrations significantly differed (P = 0.0002).

In Vivo PET Imaging

[^{18}F]FASu and [^{18}F]FSPG were evaluated in subcutaneous models of glioblastoma (U-87) and non–small cell lung cancer (A549). The expression of xCT, the light chain subunit of system x_C^-, in these tumors was confirmed ex vivo with Western blotting (Supplemental Fig. 5), which revealed a greater abundance of xCT in the A549 tumor lysate. Representative decay-corrected fused PET/CT images and biodistribution data of A549 tumor–bearing Rag2M mice are shown in Figure 4A and Table 2. Both [^{18}F]FASu and [^{18}F]FSPG gave PET images with low background uptake, high image contrast, and clear tumor visualization. Renal clearance was evident from both biodistribution data and images. [^{18}F]FASu and [^{18}F]FSPG both had high pancreatic uptake: 24.93 ± 2.92 and 17.71 ± 3.63 %ID/g, respectively. Both A549 tumor and pancreatic uptake were blocked with coinjection of the nonradioactive standard aminosuberic acid (ASu, 100 mg/kg, intravenously), indicating uptake specificity of the tracers to system x_C^- (Table 2) (*17*). Moreover, ASu coinjection resulted in measurable decreases in tumor-to-muscle, -brain, and -lung uptake ratios for [^{18}F]FASu and a decrease in tumor-to-blood ratio for [^{18}F]FSPG, as indicated in Table 2. Although [^{18}F]FSPG tumor uptake reduction with ASu coinjection was not statistically significant (P = 0.0688), it is worth noting that tumor uptake decreased more than 40% with ASu coinjection. It may also be worth noting that differences in [^{18}F]FSPG tumor-to-brain and -muscle uptake were not significant in the presence of ASu, which is in contrast to the results obtained for [^{18}F]FASu. Tumor uptake of [^{18}F]FASu and [^{18}F]FSPG was 5.00 ± 0.83 and 6.27 ± 1.32 %ID/g, respectively, although it was not significantly different between [^{18}F]FASu and [^{18}F]FSPG (Figs. 4B and 4C). [^{18}F]FSPG had a significantly greater tumor-to-brain ratio than [^{18}F]FASu ($P < 0.05$); otherwise, there were no significant differences in the biodistribution of these 2 tracers.

In the case of U-87 tumor–bearing Rag2M mice, the images (Fig. 5A) and biodistribution data (Table 3) resemble those of A549 tumor–bearing animals. Radiofluorinated amino acids [^{18}F]FASu and [^{18}F]FSPG generated good-contrast PET images in xCT-expressing glioblastoma xenografts. The 2 tracers indicated a similar biodistribution pattern in the organs and tissues that were studied (Table 3). In addition to tumor, excretory organs such as the kidneys and bladder showed uptake, indicating a renal excretion pathway (Fig. 5). Blood clearance was rapid, with 0.84 ± 0.50 and 0.59 ± 0.08 %ID/g of [^{18}F]FASu and [^{18}F]FSPG present at 1 h after injection, respectively. [^{18}F]FASu and [^{18}F]FSPG both had high pancreatic uptake, 26.42 ± 11.59 and 16.81 ± 1.38 %ID/g, respectively, because of high xCT expression in this organ (*27*). U-87 tumor uptake of [^{18}F]FASu and [^{18}F]FSPG at 1 h after injection was 6.05 ± 2.40

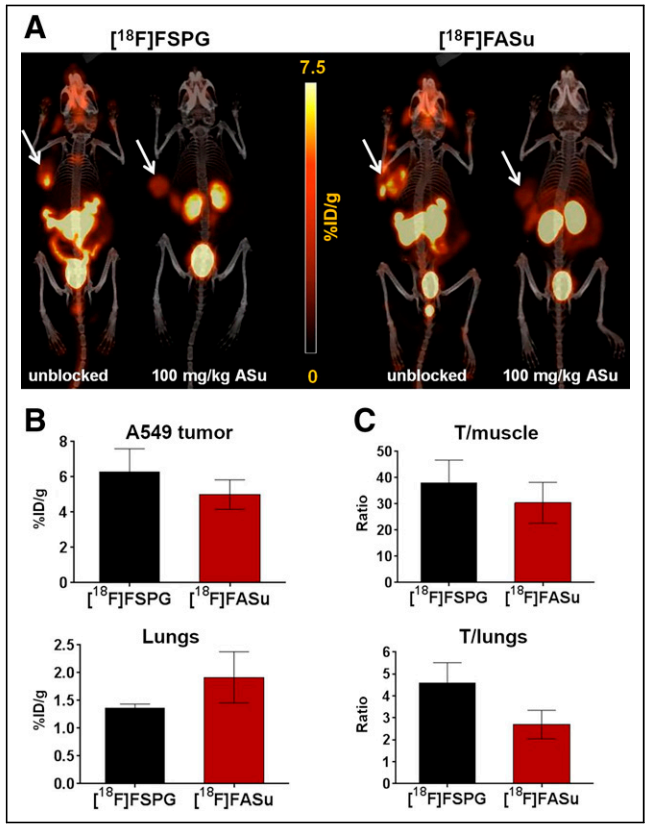

FIGURE 4. (A) Uptake of [^{18}F]FSPG and [^{18}F]FASu in A549 tumor–bearing mice at 1 h after injection with and without blocking reagent (100 mg/kg ASu). Arrows indicate location of A549 tumors on fused PET/CT maximum-intensity projection images. (B and C) Two-way ANOVA of tumor-to-muscle and tumor-to-lung ratios (C) and tumor and lung uptake (B) for [^{18}F]FSPG and [^{18}F]FASu in A549 tumor–bearing mice at 1 h after injection. P value varied for each comparison but was always >0.05. T = tumor.

TABLE 2
Biodistribution and Tumor-to-Nontarget Ratios of [^{18}F]FASu and [^{18}F]FSPG in A549 Xenograft–Bearing Rag2M Mice

	[^{18}F]FASu		[^{18}F]FSPG	
Organ	Unblocked (n = 6)	100 mg/kg ASu* (n = 4)	Unblocked (n = 6)	100 mg/kg ASu* (n = 4)
Blood	0.78 ± 0.44	0.64 ± 0.11	0.51 ± 0.08	0.55 ± 0.16
Fat	0.04 ± 0.01	0.04 ± 0.01	0.03 ± 0.01	0.02 ± 0.00
Ovaries	2.91 ± 0.50	0.91 ± 0.21†	9.13 ± 2.77	1.14 ± 0.20†
Uterus	7.96 ± 2.88	0.59 ± 0.11†	6.29 ± 2.99	0.91 ± 0.34
Small intestine	2.53 ± 0.21	0.87 ± 0.61†	2.51 ± 0.37	0.46 ± 0.13†
Stomach	0.66 ± 0.12	0.61 ± 0.42	0.85 ± 0.29	0.33 ± 0.18
Pancreas	24.93 ± 2.92	3.96 ± 1.18†	17.71 ± 3.63	3.99 ± 0.70†
Spleen	3.89 ± 2.01	1.04 ± 0.26	6.14 ± 0.84	1.02 ± 0.20†
Adrenal glands	0.65 ± 0.15	0.51 ± 0.24	0.53 ± 0.05	0.59 ± 0.16
Kidneys	13.29 ± 1.60	22.19 ± 5.85	17.49 ± 2.11	21.07 ± 10.60
Liver	0.74 ± 0.08	0.75 ± 0.17	0.63 ± 0.13	0.60 ± 0.32
Heart	0.24 ± 0.06	0.26 ± 0.05	0.16 ± 0.03	0.17 ± 0.08
Lungs	1.92 ± 0.46	2.66 ± 0.28	1.36 ± 0.07	1.00 ± 0.37
Muscle	0.15 ± 0.02	0.16 ± 0.03	0.17 ± 0.05	0.10 ± 0.03
Bone	0.56 ± 0.08	0.33 ± 0.07†	0.14 ± 0.04	0.20 ± 0.07
Brain	0.13 ± 0.02	0.09 ± 0.01	0.64 ± 0.21	0.09 ± 0.04
Tail	1.25 ± 0.20	0.75 ± 0.29	0.21 ± 0.01	0.44 ± 0.20†
A549 tumor	5.00 ± 0.83	2.04 ± 0.36†	6.27 ± 1.32	3.53 ± 0.69
Tumor/blood	7.61 ± 3.58	3.22 ± 0.58	12.36 ± 2.52	6.67 ± 1.81†
Tumor/muscle	33.18 ± 4.39	13.72 ± 4.40†	37.92 ± 9.55	39.15 ± 11.34
Tumor/lungs	2.70 ± 0.65	0.78 ± 0.20†	4.59 ± 0.92	3.77 ± 1.17
Tumor/brain	39.79 ± 6.67	23.40 ± 6.53†	52.95 ± 10.29	45.58 ± 17.86

*Blocked with coinjection of cold standard, ASu.
†Coinjection significantly reduced uptake of same organ for tracer or tumor-to-organ ratio ($P < 0.05$).
Biodistributions and ratios are at 1 h after injection. Values (%ID/g) are presented as mean ± SD.

and 11.18 ± 4.12 %ID/g, respectively. Glioblastoma xenograft uptake of [^{18}F]FSPG was significantly greater than that of [^{18}F]FASu ($P < 0.05$), as were tumor-to-muscle and tumor-to-brain uptake ratios ($P < 0.0001$; Figs. 5B and 5C). Region-of-interest analysis of the dynamic scans with [^{18}F]FASu and [^{18}F]FSPG in U-87 tumor–bearing mice showed a steady increase of tracer uptake by the tumor and a clear delineation from the background activity, as evident on the time–activity curves (Supplemental Fig. 6).

DISCUSSION

Cellular antioxidant machinery functions as a tightly controlled system, in which the purpose is to maintain an intracellular redox balance (*28,29*). Glutathione is a major endogenous nonenzymatic antioxidant involved in reactive oxygen species neutralization and containment of intracellular OS levels (*30*). Given the dependency of glutathione biosynthesis on the import of cystine into the cell, system x_C^- is considered a marker of cellular OS (*10*) and, as such, has become an appealing target for therapeutic and imaging purposes. The aim of this study was to directly compare the uptake specificity, biodistribution profile, and imaging utility of 2 tracers targeting system x_C^-, both of which have previously been reported as promising noninvasive tools for imaging of intracellular redox status.

In vitro uptake studies indicate system x_C^-–mediated uptake of both [^{18}F]FASu and [^{18}F]FSPG. We found that [^{18}F]FSPG was taken up more readily in vitro and that it had severalfold greater uptake than [^{18}F]FASu in all tested cell lines. We hypothesize that this could be because of reliance of [^{18}F]FSPG on other modes of transport across the plasma membrane, and we tested this hypothesis in a series of specificity assays in which we measured uptake of each tracer in the presence of several different amino acid transporter inhibitors (Fig. 2). In at least 2 of 3 tested cell lines, [^{18}F]FSPG uptake was significantly inhibited by PDC and L-serine ($P < 0.05$), indicating some involvement of EAATs and numerous serine transporters in the import of this tracer into these cells. Furthermore, we were able to detect the expression of EAAT3 and EAAT4 and predicted glycoproteins of EAAT1 and EAAT2 (*26*) in these cell lines (Supplemental Fig. 4), further supporting our hypothesis that there might be some reliance on EAATs in the import of [^{18}F]FSPG into these cells. An additional finding in this study was the ability of rose bengal, a known vesicular glutamate transporter inhibitor, to block transport of both [^{18}F]FASu and [^{18}F]FSPG across the plasma membrane in all cell lines studied

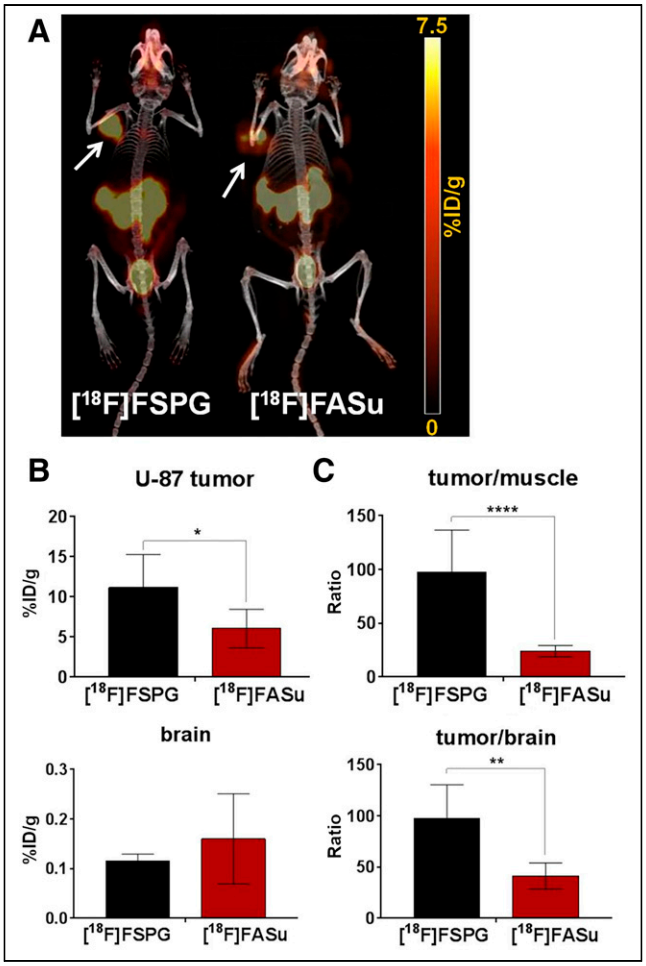

FIGURE 5. Comparative study. (A) Uptake of [^{18}F]FSPG and [^{18}F]FASu in U-87 tumor–bearing mice at 1 h after injection. Arrows indicate location of U-87 tumors on fused PET/CT maximum-intensity projection images. (B and C) Two-way ANOVA of tumor-to-muscle and tumor-to brain ratios (C) and tumor and brain uptake (B) for [^{18}F]FSPG and [^{18}F]FASu in U-87 tumor–bearing mice at 1 h after injection. *$P < 0.05$. **$P < 0.01$. ****$P < 0.0001$.

($P < 0.01$; Fig. 2). When coincubated with either one of these 2 radiotracers, rose bengal caused a dose-dependent reduction in intracellular tracer content (Supplemental Fig. 3). Only 10 μM rose bengal was sufficient to prevent greater than 90% of activity from entering A549 cells, which is equivalent to the percentage inhibition achieved by 1 mM sulfasalazine in this study. With these results, the finding that rose bengal inhibits system x_C^- raises the prospect that this compound may induce a therapeutic response (*31,32*) via glutathione depletion, thus sensitizing the target tissue to other chemotherapeutics (*6,33–35*).

[^{18}F]FASu and [^{18}F]FSPG biodistribution and imaging potential was tested in mice bearing U-87 and A549 xenografts. These 2 tumor models were selected for the in vivo experiments because of their disparate uptake pattern in vitro. U-87 cells were on the lower end of the uptake spectra of both tracers, and no increase in blocked uptake of either tracer was evident in vitro. The lung cancer cells, A549, conversely, demonstrated high in vitro uptake of both radiotracers and increasing uptake over time despite oversaturation with sulfasalazine, which is a system x_C^- inhibitor.

TABLE 3
Biodistribution and Tumor-to-Nontarget Ratios of [^{18}F]FASu and [^{18}F]FSPG in U-87 Xenograft–Bearing Rag2M Mice

Organ	[^{18}F]FASu	[^{18}F]FSPG
Organ	Unblocked ($n \geq 4$)	Unblocked ($n \geq 4$)
Blood	0.84 ± 0.50	0.59 ± 0.08
Fat	0.04 ± 0.02	0.02 ± 0.00
Ovaries	3.07 ± 1.48	5.62 ± 4.09
Uterus	5.97 ± 3.08	5.07 ± 0.73
Small intestine	1.83 ± 0.64	2.18 ± 0.40
Stomach	1.66 ± 1.13	1.08 ± 0.73
Pancreas	26.42 ± 11.59	16.81 ± 1.38
Spleen	4.47 ± 1.65	6.58 ± 1.58
Adrenal glands	0.46 ± 0.15	0.55 ± 0.05
Kidneys	17.79 ± 7.20	17.92 ± 2.49
Liver	0.95 ± 0.44	0.59 ± 0.14
Heart	0.36 ± 0.21	0.17 ± 0.01
Lungs	3.41 ± 2.20	1.39 ± 0.16
Muscle	0.26 ± 0.11	0.12 ± 0.02
Bone	0.76 ± 0.46	0.76 ± 0.17
Brain	0.16 ± 0.09	0.12 ± 0.01
Tail	1.82 ± 0.90	1.26 ± 0.24
U-87 tumor	6.05 ± 2.40	11.18 ± 4.12
Tumor/blood	7.96 ± 2.81	18.67 ± 6.30
Tumor/muscle	24.08 ± 5.20	97.86 ± 38.99
Tumor/lungs	1.96 ± 0.51	8.04 ± 2.60
Tumor/brain	41.30 ± 12.73	97.22 ± 33.15

Biodistributions and ratios are at 1 h after injection. Values (%ID/g) are presented as mean ± SD.

In contrast to the in vitro uptake, [^{18}F]FASu and [^{18}F]FSPG have similar biodistribution profiles and excretion pathways, irrespective of the tumor inoculated (A549 or U-87; Tables 2 and 3). Both tracers exhibited low background uptake and moderate to high tumor-to-blood, tumor-to-brain, and tumor-to-muscle ratios. The principal difference between [^{18}F]FASu and [^{18}F]FSPG was found in the greater in vivo tumor uptake of the latter, with significantly greater uptake in the U-87 tumor (Fig. 5B; $P < 0.05$) yet nonsignificantly greater uptake in A549 tumors (Fig. 4B; $P = 0.79$), despite greater xCT expression in these tumors (Supplemental Fig. 5). This may be an indication that [^{18}F]FSPG is transported into the cells by the action of alternative transporters, including the EAATs, or system x_{AG}^-, in addition to system x_C^- (*36*). Moreover, an early report on the specificity of [^{18}F]FSPG by Koglin et al. (*12*) demonstrated that, although [^{18}F]FSPG does predominantly use system x_C^- to enter cells, both L-cystine and L-glutamate achieved higher levels of tracer uptake inhibition than a potent system x_C^- inhibitor, *p*-carboxy-phenylglycine, indicating that [^{18}F]FSPG may be a suitable substrate for other AATs that include L-glutamate or L-cystine as substrates, such as EAATs (EAAT1, EAAT2, EAAT4, and EAAT5 for L-glutamate and EAAT3 for both) (*24*). The authors also reported observing a minor competition with either L- or

D-aspartate, both of which are substrates along with L-glutamate for the EAAT family members 1–5 (*24*). Webster et al. (*10*) performed a similar in vitro uptake inhibition uptake assay with [^{18}F]FASu, and in their study, sulfasalazine was more effective in blocking tracer uptake than L-glutamate, signifying a preference of [^{18}F]FASu for system x_C^-. The authors reported observing little effect of D-aspartate on [^{3}H]ASu, [^{3}H]Glu, and [^{3}H]Leu uptake, which is in agreement with our finding reported here that [^{18}F]FASu uptake was not affected by the system x_{AG}^- inhibitor PDC.

Notwithstanding the data presented here, we are aware of other potential explanations for the in vitro uptake fluctuations of [^{18}F]FSPG involving the complex interplay between amino acid transporters and their respective substrates. Inhibition of EAATs has been previously shown to alter intracellular glutamate levels, which are known to affect system x_C^- activity (*37*). Given that fluctuations in intracellular glutamate levels also affect [^{18}F]FSPG retention (*38*) because of system x_C^-–mediated exchange, this phenomenon may account for changes in cell retention together with alternative transport mechanisms. Moreover, serine is a precursor for the biosynthesis of cysteine, the levels of which have been shown to affect [^{18}F]FSPG retention in cells through x_C^- exchange (*38*).

Several recent studies have examined the potential use of [^{18}F]FSPG and [^{18}F]FASu for measuring intracellular redox status. McCormick et al. found that in vitro [^{18}F]FSPG uptake in ovarian cancer cells was sensitive to an elevation in glutathione biosynthesis after drug-induced OS (*38*). Our group recently reported a positive correlation between in vitro [^{18}F]FASu uptake and intracellular glutathione fluctuations in breast cancer models caused by radiation- and diethylmaleate-induced OS (*17*). Despite the methodic and detailed approach taken in previous studies, a side-by-side study comparing [^{18}F]FASu and [^{18}F]FSPG in the same cancer model became warranted to better understand the subtleties in tracer behavior. The data presented here suggest that the degree of non–system x_C^- uptake may vary depending on the cancer model studied and the mode of action of the OS-inducing drug used. Other reports testify to the emerging (poor) prognostic significance of xCT/*SLC7A11* overexpression in several different malignancies, including non–small cell lung cancer (*39*), laryngeal squamous cell carcinoma (*40*), glioblastoma (*41,42*), hepatocellular carcinoma (*43*), colorectal cancer (*44,45*), and acute myeloid leukemia (*46,47*). Additional studies speak to the increasing potential of using xCT-targeting therapeutics to sensitize cancers to chemotherapy or radiation therapy (*6,33–35,48–50*). Therefore, early identification of xCT-expressing tumors would help with patient stratification, treatment plan development, and therapeutic monitoring and intervention because xCT has been recognized as an emerging therapeutic or adjuvant target.

The main objective of this work was to compare the 2 tracers with respect to their specificity for the target transporter and tumor visualization potential. [^{18}F]FSPG is currently in use in pilot clinical studies (*51–53*) and is showing promise as a marker of therapeutic response in the preclinical setting in high-grade serous ovarian cancer models (*54*). [^{18}F]FASu performed as well as [^{18}F]FSPG as an in vivo oncologic imaging agent in a preclinical setting and may warrant further consideration for clinical use.

CONCLUSION

We found that [^{18}F]FSPG is taken up more readily in vitro by all cell lines tested, whereas ex vivo biodistribution was generally equivalent between [^{18}F]FSPG and [^{18}F]FASu, with the exception of greater [^{18}F]FSPG uptake in glioblastoma xenografts. This study examined the participation of alternative AATs, such as system x_{AG}^-, in the transport of both tracers. Nevertheless, we found that [^{18}F]FSPG and [^{18}F]FASu have comparable biodistribution and tumor-imaging ability in vivo, supporting the further pursuit of either tracer for non-[^{18}F]FDG oncologic imaging.

DISCLOSURE

This work was supported by the CIHR (grants 201403COP and 329895). TRIUMF receives federal funding via a contribution agreement with the National Research Council of Canada. This work was supported in part by the BC Leading Edge Endowment Fund. Milena Colovic received support from an NSERC CREATE IsoSiM fellowship, grant 448110, competition year 2014. No other potential conflict of interest relevant to this article was reported.

ACKNOWLEDGMENTS

We thank the TRIUMF TR13 cyclotron team, in particular David Prevost, Linda Graham, and Samuel Varah, for technical assistance.

KEY POINTS

QUESTION: How do the 2 system x_C^- imaging agents, [^{18}F]FASu and [^{18}F]FSPG, compare with respect to their uptake specificity and tumor imaging potential?

PERTINENT FINDINGS: Our in vitro specificity assays indicated greater overall uptake of [^{18}F]FSPG than of [^{18}F]FASu but also potential participation of other AA transporters. Moreover, we found that rose bengal inhibited uptake of both tracers in vitro. In preclinical subjects, however, both tracers were successful at visualizing glioma (U-87) and lung cancer (A549) xenografts and had comparable tumor uptake and pharmacokinetics.

IMPLICATIONS FOR PATIENT CARE: [^{18}F]FASu and [^{18}F]FSPG are redox PET tracers that, when translated into the clinic, have the potential to serve as indicators of the redox state of the lesion, companion diagnostics, and, potentially, patient prognosis.

REFERENCES

1. Reuter S, Gupta SC, Chaturvedi MM, Aggarwal BB. Oxidative stress, inflammation, and cancer: how are they linked? *Free Radic Biol Med.* 2010;49:1603–1616.
2. Gorrini C, Harris IS, Mak TW. Modulation of oxidative stress as an anticancer strategy. *Nat Rev Drug Discov.* 2013;12:931–947.
3. Bridges RJ, Natale NR, Patel SA. System x_c^- cystine/glutamate antiporter: an update on molecular pharmacology and roles within the CNS. *Br J Pharmacol.* 2012;165:20–34.
4. Conrad M, Sato H. The oxidative stress-inducible cystine/glutamate antiporter, system x_c^-: cystine supplier and beyond. *Amino Acids.* 2012;42:231–246.
5. Sato H, Ishii T, Kuriyama-Matsumura K, et al. Effect of oxygen on induction of the cystine transporter by bacterial lipopolysaccharide in mouse peritoneal macrophages. *J Biol Chem.* 2002;276:10407–10412.
6. Timmerman LA, Holton T, Yuneva M, et al. Glutamine sensitivity analysis identifies the xCT antiporter as a common triple negative breast tumor therapeutic target. *Cancer Cell.* 2013;24:450–465.
7. Nakanishi T, Tamai I. Solute carrier transporters as targets for drug delivery and pharmacological intervention for chemotherapy. *J Pharm Sci.* 2011;100:3731–3750.
8. Ganapathy V, Thangaraju M, Prasad PD. Nutrient transporters in cancer: relevance to Warburg hypothesis and beyond. *Pharmacol Ther.* 2009;121:29–40.
9. Yang H, Miao Q, Johnson BF, et al. A simple route to [^{11}C]N-Me labeling of aminosuberic acid for proof of feasibility imaging of the x_C^- transporter. *Bioorg Med Chem Lett.* 2014;24:5512–5515.

10. Webster JM, Morton CA, Johnson BF, et al. Functional imaging of oxidative stress with a novel PET imaging agent, ^{18}F-5-fluoro-L-aminosuberic acid. *J Nucl Med.* 2014;55:657–664.
11. Krasikova RN, Kuznetsova OF, Fedorova OS, et al. 4-[^{18}F]fluoroglutamic acid (BAY 85-8050), a new amino acid radiotracer for PET imaging of tumors: synthesis and in vitro characterization. *J Med Chem.* 2011;54:406–410.
12. Koglin N, Mueller A, Berndt M, et al. Specific PET imaging of x_C^- transporter activity using a ^{18}F-labeled glutamate derivative reveals a dominant pathway in tumor metabolism. *Clin Cancer Res.* 2011;17:6000–6011.
13. Beinat C, Gowrishankar G, Shen B, et al. The characterization of ^{18}F-hGTS13 for molecular imaging of x_C^- transporter activity with positron emission tomography. *J Nucl Med.* 2019;60:1812–1817.
14. Greenwood HE, Edwards R, Koglin N, et al. Radiotracer stereochemistry affects substrate affinity and kinetics for improved imaging of system x_C^- in tumors. *Theranostics.* 2022;12:1921–1936.
15. ClinicalTrial.gov website. https://clinicaltrials.gov/ct2/results?cond=cancer&term=fspg&cntry=&state=&city=&dist=. Published November 2015. Accessed April 12, 2023.
16. Yang H, Jenni S, Colovic M, et al. ^{18}F-5-fluoroaminosuberic acid as a potential tracer to gauge oxidative stress in breast cancer models. *J Nucl Med.* 2017; 58:367–373.
17. Čolović M, Yang H, Merkens H, Colpo N, Bénard F, Schaffer P. Non-invasive use of positron emission tomography to monitor diethyl maleate and radiation-induced changes in system x_C^- activity in breast cancer. *Mol Imaging Biol.* 2019; 21:1107–1116.
18. Yang H, Tam B, Čolović M, et al. Addressing chirality in the structure and synthesis of [^{18}F]5-fluoroaminosuberic acid ([^{18}F]FASu). *Chemistry.* 2017;23: 11100–11107.
19. Lewerenz J, Klein M, Methner A. Cooperative action of glutamate transporters and cystine/glutamate antiporter system x_c^- protects from oxidative glutamate toxicity. *J Neurochem.* 2006;98:916–925.
20. Neale SA, Copeland CS, Salt TE. Effect of VGLUT inhibitors on glutamatergic synaptic transmission in the rodent hippocampus and prefrontal cortex. *Neurochem Int.* 2014;73:159–165.
21. Haase C, Bergmann R, Fuechtner F, Hoepping A, Pietzsch J. L-type amino acid transporters LAT1 and LAT4 in cancer: uptake of 3-O-methyl-6-^{18}F-fluoro-L-dopa in human adenocarcinoma and squamous cell carcinoma in vitro and in vivo. *J Nucl Med.* 2007;48:2063–2071.
22. Kim CS, Cho SH, Chun HS, Lee SY, Ndou HE. BCH, an inhibitor of system L amino acid transporters, induces apoptosis in cancer cells. *Biol Pharm Bull.* 2008; 31:1096–1100.
23. Wagner CA, Lang F, Broer S. Function and structure of heterodimeric amino acid transporters. *Am J Physiol Cell Physiol.* 2001;281:C1077–C1093.
24. Bröer S, Bröer A. Amino acid homeostasis and signalling in mammalian cells and organisms. *Biochem J.* 2017;474:1935–1963.
25. Pietrancosta N, Kessler A, Favre-Besse FC, et al. Rose Bengal analogs and vesicular glutamate transporters (VGLUTs). *Bioorg Med Chem.* 2010;18:6922–6933.
26. Parkin GM, Udawela M, Gibbons A, Dean B. Glutamate transporters, EAAT1 and EAAT2, are potentially important in the pathophysiology and treatment of schizophrenia and affective disorders. *World J Psychiatry.* 2018;8:51–63.
27. Lewerenz J, Hewett SJ, Huang Y, et al. The cystine/glutamate antiporter system x_c^- in health and disease: from molecular mechanisms to novel therapeutic opportunities. *Antioxid Redox Signal.* 2013;18:522–555.
28. Phaniendra A, Jestadi DB, Periyasamy L. Free radicals: properties, sources, targets, and their implication in various diseases. *Indian J Clin Biochem.* 2015;30:11–26.
29. Cairns RA, Harris IS, Mak TW. Regulation of cancer cell metabolism. *Nat Rev Cancer.* 2011;11:85–95.
30. Trachootham D, Alexandre J, Huang P. Targeting cancer cells by ROS-mediated mechanisms: a radical therapeutic approach? *Nat Rev Drug Discov.* 2009;8:579–591.
31. Ross MI. Intralesional therapy with PV-10 (Rose Bengal) for in-transit melanoma. *J Surg Oncol.* 2014;109:314–319.
32. Read TA, Smith A, Thomas J, et al. Intralesional PV-10 for the treatment of in-transit melanoma metastases: results of a prospective, non-randomized, single center study. *J Surg Oncol.* 2018;117:579–587.
33. Daher B, Parks SK, Durivault J, et al. Genetic ablation of the cystine transporter xCT in PDAC cells inhibits mTORC1, growth, survival, and tumor formation via nutrient and oxidative stresses. *Cancer Res.* 2019;79:3877–3890.
34. Sato M, Kusumi R, Hamashima S, et al. The ferroptosis inducer erastin irreversibly inhibits system x_c^- and synergizes with cisplatin to increase cisplatin's cytotoxicity in cancer cells. *Sci Rep.* 2018;8:968.
35. Yoshikawa M, Tsuchihashi K, Ishimoto T, et al. XCT inhibition depletes CD44v-expressing tumor cells that are resistant to EGFR-targeted therapy in head and neck squamous cell carcinoma. *Cancer Res.* 2013;73:1855–1866.
36. Hyde R, Taylor PM, Hundal HS. Amino acid transporters: roles in amino acid sensing and signalling in animal cells. *Biochem J.* 2003;373:1–18.
37. Bannai S, Ishii T. A novel function of glutamine in cell culture: utilization of glutamine for the uptake of cystine in human fibroblasts. *J Cell Physiol.* 1988;137: 360–366.
38. McCormick PN, Greenwood HE, Glaser M, et al. Assessment of tumor redox status through (S)-4-(3-[^{18}F]fluoropropyl)-L-glutamic acid PET imaging of system x_C^- activity. *Cancer Res.* 2019;79:853–863.
39. Ji X, Qian J, Rahman SMJ, et al. xCT (SLC7A11)-mediated metabolic reprogramming promotes non-small cell lung cancer progression. *Oncogene.* 2018;37:5007–5019.
40. Ma Z, Zhang H, Lian M, et al. SLC7A11, a component of cysteine/glutamate transporter, is a novel biomarker for the diagnosis and prognosis in laryngeal squamous cell carcinoma. *Oncol Rep.* 2017;38:3019–3029.
41. Takeuchi S, Wada K, Toyooka T, et al. Increased xCT expression correlates with tumor invasion and outcome in patients with glioblastomas. *Neurosurgery.* 2013; 72:33–41.
42. Robert SM, Buckingham SC, Campbell SL, et al. SLC7A11 expression is associated with seizures, predicts poor survival in patients with malignant glioma. *Sci Transl Med.* 2015;7:289ra86.
43. Zhang L, Huang Y, Ling J, et al. Overexpression of SLC7A11: a novel oncogene and an indicator of unfavorable prognosis for liver carcinoma. *Future Oncol.* 2018; 14:927–936.
44. Lim JKM, Delaidelli A, Minaker SW, et al. Cystine/glutamate antiporter xCT (SLC7A11) facilitates oncogenic RAS transformation by preserving intracellular redox balance. *Proc Natl Acad Sci USA.* 2019;116:9433–9442.
45. Sugano K, Maeda K, Ohtani H, Nagahara H, Shibutani M, Hirakawa K. Expression of xCT as a predictor of disease recurrence in patients with colorectal cancer. *Anticancer Res.* 2015;35:677–682.
46. Zhao X, Li Y, Wu H. A novel scoring system for acute myeloid leukemia risk assessment based on the expression levels of six genes. *Int J Mol Med.* 2018;42: 1495–1507.
47. Lin W, Wang C, Liu G, et al. SLC7A11/xCT in cancer: biological functions and therapeutic implications. *Am J Cancer Res.* 2020;10:3106–3126.
48. Wada F, Koga H, Akiba J, et al. High expression of CD44v9 and xCT in chemoresistant hepatocellular carcinoma: potential targets by sulfasalazine. *Cancer Sci.* 2018;109:2801–2810.
49. Polewski MD, Reveron-Thornton RF, Cherryholmes GA, Marinov GK, Aboody KS. SLC7A11 overexpression in glioblastoma is associated with increased cancer stem cell-like properties. *Stem Cells Dev.* 2017;26:1236–1246.
50. Cobler L, Zhang H, Suri P, Park C, Timmerman LA. xCT inhibition sensitizes tumors to γ-radiation via glutathione reduction. *Oncotarget.* 2018;9:32280–32297.
51. Baek S, Choi CM, Ahn S, et al. Exploratory clinical trial of (4S)-4-(3-[^{18}F]fluoropropyl)-L-glutamate for imaging x_C^- transporter using positron emission tomography in patients with non-small cell lung or breast cancer. *Clin Cancer Res.* 2012; 18:5427–5437.
52. Baek S, Mueller A, Lim Y, et al. (4S)-4-(3-^{18}F-fluoropropyl)-L-glutamate for imaging of x_C^- transporter activity in hepatocellular carcinoma using PET: preclinical and exploratory clinical studies. *J Nucl Med.* 2013;54:117–123.
53. Kavanaugh G, Williams J, Morris AS, et al. Utility of [^{18}F]FSPG PET to image hepatocellular carcinoma: first clinical evaluation in a US population. *Mol Imaging Biol.* 2016;18:924–934.
54. Greenwood HE, McCormick PN, Gendron T, et al. Measurement of tumor antioxidant capacity and prediction of chemotherapy resistance in preclinical models of ovarian cancer by positron emission tomography. *Clin Cancer Res.* 2019;25: 2471–2482.